 https://doi.org/10.3311/PPee.20517

Periodica Polytechnica Electrical Engineering and Computer Science, 67(2), pp. 204–215, 2023

New Modeling and Improved Current Control Strategy to Eliminate the Impact of Synchronization Method and Parks Transformation for Grid-connected Four-leg PWM Inverter

Ala Addin Mohammed Al-Dwa[1], Ali Chebabhi[1*], Mabrouk Defdaf[1], Anwar Guessabi[2]

[1] EE Laboratory, Department of Electrical Engineering, Faculty of Technology, University of M'sila, 28000 M'sila, P.O.B. 166, M'Sila, Algeria
[2] LAS Laboratory, Faculty of Technology, Ferhat Abbas University Setif 1, Campus El Bez, 19137 Setif, Algeria
[*] Corresponding author, e-mail: ali.chebabhi@univ-msila.dz

Received: 23 May 2022, Accepted: 13 December 2022, Published online: 17 February 2023

Abstract

The synchronization method's ability is one of the fundamental guarantees for the stability and accuracy of injected current control for grid-connected converter-based distribution resources. These synchronization methods, such as phase locked loop (PLL), are generally based on Park transformation and grid voltage regulation, which may affect an unstable phenomenon under distortion and unbalanced grid voltage conditions and result in more computational complexity. In this present paper, analogous to the traditional voltage-oriented control strategy (VOC) in the synchronous rotating frame (dq0-frame) based on PLL and Parks transformation, an improved voltage-oriented control strategy (IVOC) without synchronization methods and Parks transformation is proposed for grid-connected four-leg inverters (GC-FLVSI) to achieve accurate current control with high-quality performance in the dq0-frame. This proposed strategy is not only used for controlling the GC-FLVSI but also to provide the module of GC-FLVSI in the dq0-frame based on the instantaneous active and reactive powers theory (DPC). The proposed IVOC strategy has the same properties and identical performance as the traditional VOC when the grid phase angle is correctly detected by any synchronization method, with the advantages of both traditional DPC and VOC at the same time. In order to validate the superiority and excellent dynamic and steady-state performances of the proposed IVOC strategy in comparison with the traditional VOC strategy, some simulation scenarios using MATLAB/Simulink under different operations and grid conditions have been performed and presented.

Keywords

grid-connected four-leg inverters (GC-FLVSI), improved voltage oriented control strategy (IVOC), synchronous rotating frame (dq0-frame), dq0-axes inject current control, dynamic responses and steady-state performances

1 Introduction

It is well known that in recent years, the worldwide demand for electrical energy has seen a significant increase due to the large expansion of energy demands for domestic and industrial applications [1]. For this purpose, considerable attention and challenge is directed towards renewable energy resources (RER) that are inexhaustible and spotless, including solar and wind energy technology [2, 3]. Because of its high reliability, efficiency, low total harmonic distortion (THD), fast dynamics, high-power applications, and bidirectional power flow, the three-phase three-leg PWM voltage source inverter (VSI) is the key device and the most common choice for interfacing, controlling, and delivering renewable energy [4–6].

A PWM VSI-RER system can operate in two modes: 1) grid-connected VSI systems (GC-VSIs) [6] and 2) stand-alone systems (SAVSIs) [7]. The GC-VSI operation mode system is the focus of this work and is used for low and high power applications to transform, control, and inject the maximal power from RER systems into the grid with high power quality under any climatic change [8, 9]. However, for many GC-VSI applications, the classical three-leg PWM VSI may not be a perfect option due to the unbalanced single-phase nonlinear loads connected to the main grid or non-symmetrical grid impedance [10, 11]. In addition, if the three-leg PWM VSI is connected to an unbalanced grid voltage, an uncontrolled third-order harmonic

Cite this article as: Al-Dwa, A. A. M., Chebabhi, A., Defdaf, M., Guessabi, A. "New Modeling and Improved Current Control Strategy to Eliminate the Impact of Synchronization Method and Parks Transformation for Grid-connected Four-leg PWM Inverter", Periodica Polytechnica Electrical Engineering and Computer Science, 67(2), pp. 204–215, 2023. https://doi.org/10.3311/PPee.20517

appears as an oscillation on the grid currents. This effects the RER system operations, which leads to further damage to the three-leg PWM VSI power switches and augments the THD of the grid currents [12]. As a result, the use of four wire grid-connected four-leg PWM VSIs (GC-FLVSIs) is mandatory to preserve balanced sinusoidal grid voltages and currents under all loading and grid conditions, including unbalanced loads, voltages, and other disturbances [13–15], which provides a zero-sequence current channel and preserves the ability to handle all unbalanced problems [16, 17]. These FLVSIs are frequently used in grid-connected [14, 15], active filters (AF) [17], and distributed static compensators (DSTATCOM) [18, 19].

On the other hand, the performance of the GC-FLVSI depends strongly on the selected control strategy and its three current inner controllers as well. The voltage-oriented control (VOC) strategies in the dq0-frame are the most popular control strategies in power converter control. They provide a time-invariant FLVSI mathematical model in the dq0-frame, and its control becomes very similar to that of DC/DC power converter control, which can also be readily controlled using diverse controllers [20–25]. These VOC strategies that have been developed for GC-VSI have the same purpose with various structures.

The grid synchronization method and Park transformation are two highly significant and necessary peculiarities in these control strategies and are used for properly deriving the system time-invariant model in dq0-frame, synchronizing VSIs to the grid, and controlling the GC-VSIs. Furthermore, the grid synchronization method has an important role in VOC strategies, being applied in diverse Park's transformations and inverse Park's transformations to precisely determine the grid voltage phase angle and consequently provide the accuracy of the grid current closed-loop control in GC-VSI [26, 27].

So far, the phase-locked loop (PLL) has been the most commonly used synchronization method in traditional VOC strategies, providing faster control dynamics as its bandwidth is increased and the proportional and integral parameters of its closed-loop control are increased [26–28]. However, the slow dynamics of the PLL increases the difficulty of grid voltage frequency or phase angle detection, which affects the accuracy control performance and dynamics responses of the grid-connected converter systems, and the larger bandwidth of the PLL and the parameters of its closed-loop control may affect an unstable phenomenon due to the distortion and unbalanced grid voltage conditions and make the high-frequency resonance more probable to occur due to a smaller phase margin [28, 29]. Furthermore, the inherent complexity of the PLLs and the various Park transformations, as well as their inverse use in these control strategies, adds a high computational burden [30].

So, to provide high control performance and better dynamic responses with lower computational complexity under voltage distortion and unbalanced conditions, several control strategies without synchronization methods have been proposed for synchronizing and controlling the grid-connected converters in recent literature [31]. Among them, the Direct Power Control strategy based on space vector pulse width modulation (DPC-SVPWM) has been researched as an alternative control strategy to directly control the real and reactive powers without using any synchronization method [32, 33]. It can reduce power fluctuations while providing accurate control performance and better dynamic responses. Another DPC with fixed switching frequency control strategies, DPC based model predictive control strategies MP-DPC with system uncertainties, multivariable, and nonlinearities consideration has been proposed in [34–36]. These strategies provide stable and fast dynamic responses and fixed switching frequencies, but they may result in more computational complexity.

Other current control strategies in the dq-frame without a synchronization method have been proposed, which have better control performance and dynamic responses under grid voltage distortion conditions. The VOC strategy based on coordinate transformation for three-phase AC/DC converters [37], the VOC-based DPC for GC-VSIs [23], and the VOC-based Grid Voltage-Modulated (GVM-VOC) for VSIs and DFIG [38, 39] are some examples. These control strategies based on both DPC and traditional VOC concepts provide a linearly time-invariant system in the dq0-frame based on the instantaneous active and reactive powers theory, while having the same properties and control circuit structure as the traditional VOC when the grid voltage phase angle is correctly detected. Furthermore, it has both DPC and traditional VOC advantages at the same time, as well as better control performance with lower computational complexity.

In this work, we propose an improved VOC control strategy (IVOC) combining the DPC-3DSVPWM strategy and the traditional VOC strategy in the dq0-frame without using both the synchronization method and the Parks transformation for GC-FLVSI under unbalanced grid voltage conditions. The proposed IVOC control strategy synchronizes the FLVSI to the grid based on DPC theory,

which has high-quality performance due to direct inject current control in the dq0-frame and improved control performance under the slow dynamics of PLL. The four-leg topology is adopted for its ability to provide zero-sequence current regulation and thus avoid voltage fluctuation at the point of common coupling (PCC). In this work, the transient responses and steady state performance of the proposed IVOC strategy for GC-FLVSI are evaluated and compared with those based on the traditional VOC strategy in terms of grid current harmonics, zero-sequence current mitigation, neutral current reduction, and robustness versus system uncertainties and parameter mismatches or variations. The proposed IVOC strategy for GC-FLVSI illustrates satisfactory results for all the previous performance indicators, which demonstrates the superiority and effectiveness of the proposed strategy.

2 Modeling of three-phase four leg PWM inverter

In this section, in the first part, a traditional modeling of GC-FLVSI in the dq0-frame based on Park transformation and the PLL system is presented. This model is determined based on DPC modeling without the synchronization method and the Parks transformation in the second part.

The structure of the three-phase FLVSI topology connected to the grid is depicted in Fig. 1, in which magnetically independent filter inductors (L_{fabcn}) with internal resistors (R_{fabcn}) are used to attenuate the output currents high-frequency switching ripple. The grid is modeled by three sinusoidal voltages e_{abc} and a grid neutral line in series with four inductors (L_{gabcn}) having internal resistances (R_{gabcn}) and tied up with the FLVSI at the point of common coupling (PCC). The FLVSI inject currents and output voltages are denoted as v_{fabc} and i_{fabc}, respectively. i_{fn} and I_{dc} are the neutral line current and FLVSI input DC current, respectively. The voltages at the point of common coupling (PCC) are denoted by v_{gabc}.

2.1 Traditional GCFLVSI modeling based Park transformation and PLL system in dq0-frame

Accordingly, the three-phase GCFLVSI average model that describes the output voltage in the *abc*-reference-frame is presented in Eq. (1).

$$V_f = V_g + L_{fa}\frac{\mathrm{d}I_f}{\mathrm{d}t} + R_f I_f + R_{fn} i_n + L_{fn}\frac{\mathrm{d}i_n}{\mathrm{d}t} \tag{1}$$

The dynamic equations of GC-FLVSI inject currents in *abc*-reference-frame are expressed as:

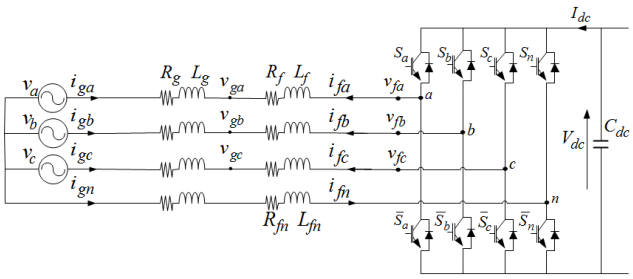

Fig. 1 Structure of the four leg PWM VSI connected to the grid

$$\begin{cases} L_{fa}\dfrac{\mathrm{d}i_{fa}}{\mathrm{d}t} = -v_{ga} - R_{fa}i_{fa} + v_{fa} - R_{fn}i_{fn} - L_{fn}\dfrac{\mathrm{d}i_{fn}}{\mathrm{d}t} \\ L_{fb}\dfrac{\mathrm{d}i_{fb}}{\mathrm{d}t} = -v_{gb} - R_{fb}i_{fb} + v_{fb} - R_{fn}i_{fn} - L_{fn}\dfrac{\mathrm{d}i_{fn}}{\mathrm{d}t} \\ L_{fc}\dfrac{\mathrm{d}i_{fc}}{\mathrm{d}t} = -v_{gc} - R_{fc}i_{fc} + v_{fc} - R_{fn}i_{fn} - L_{fn}\dfrac{\mathrm{d}i_{fn}}{\mathrm{d}t} \end{cases}. \tag{2}$$

Using Park transformation based on the PLL system and after several mathematical operations, the system Eq. (1) is expressed in the dq0-frame as:

$$\begin{cases} \dfrac{\mathrm{d}i_{fd}}{\mathrm{d}t} = -\dfrac{R_f}{L_f}i_{fd} + \omega i_{fq} - \dfrac{v_{gd}}{L_f} + \dfrac{v_{fd}}{L_f} \\ \dfrac{\mathrm{d}i_{fq}}{\mathrm{d}t} = -\dfrac{R_f}{L_f}i_{fq} - \omega i_{fd} - \dfrac{v_{gq}}{L_f} + \dfrac{v_{fq}}{L_f} \\ \dfrac{\mathrm{d}i_{f0}}{\mathrm{d}t} = -\dfrac{(R_f + 3R_n)}{(L_f + 3L_n)}i_{f0} - \dfrac{v_{g0} + v_{f0}}{(L_f + 3L_n)} \end{cases}, \tag{3}$$

where i_{fd}, i_{fq}, and i_{f0} are the d-axis, q-axis, and 0-axis (zero-sequence current) FLVSI inject currents, respectively; v_{fd}, v_{fq}, and v_{f0} are the d-axis, q-axis, and 0-axis (zero-sequence voltage) FLVSI output voltages, respectively; and ω the grid angular frequency.

The zero-sequence current i_{f0} is given through the inject currents (i_{fabc}) and the neutral input current (i_{fn}) as:

$$i_{f0} = \frac{1}{\sqrt{3}}\left(i_{fa} + i_{fb} + i_{fc}\right) = \frac{1}{\sqrt{3}}i_{fn}. \tag{4}$$

2.2 Grid connected four-leg PWM VSI modeling in dq0-frame based power theory

Using the Concordia transformation of the system Eq. (1), the dynamic equations of GCFLVSI in the stationary reference frame (αβ0-frame) are given as follows:

$$\begin{cases} \dfrac{\mathrm{d}i_{f\alpha}}{\mathrm{d}t} = -\dfrac{R_f}{L_f}i_{f\alpha} - \dfrac{v_{g\alpha}}{L_f} + \dfrac{v_{f\alpha}}{L_f} \\ \dfrac{\mathrm{d}i_{f\beta}}{\mathrm{d}t} = -\dfrac{R_f}{L_f}i_{f\beta} - \dfrac{v_{g\beta}}{L_f} + \dfrac{v_{f\beta}}{L_f} \\ \dfrac{\mathrm{d}i_{f0}}{\mathrm{d}t} = -\dfrac{(R_f + 3R_n)}{(L_f + 3L_n)}i_{f0} - \dfrac{v_{g0} + v_{f0}}{(L_f + 3L_n)} \end{cases}, \tag{5}$$

where $i_{f\alpha\beta0}$, $v_{f\alpha\beta0}$, and $v_{g\alpha\beta0}$ indicate the FLVSI inject currents, output voltages, and grid voltages in the αβ0-frame, respectively.

The grid active and reactive powers (p_g and q_g) can be expressed in the *abc*-frame as follows [6]:

$$\begin{cases} p_g = v_{ga} i_{fa} + v_{gb} i_{fb} + v_{gc} i_{fc} \\ q_g = \sqrt{\frac{1}{3}} \left[(v_{gb} - v_{gc}) i_{fa} + (v_{gc} - v_{ga}) i_{fb} + (v_{ga} - v_{gb}) i_{fc} \right] \end{cases}. \quad (6)$$

These powers can be expressed in the αβ0-frame as:

$$\begin{cases} p_g = v_{g\alpha} i_{f\alpha} + v_{g\beta} i_{f\beta} + v_{g0} i_{f0} \\ q_g = v_{g\beta} i_{f\alpha} - v_{g\alpha} i_{f\beta} \end{cases}. \quad (7)$$

Using the derivative of Eq. (7), the inject power dynamics can be obtained as:

$$\begin{cases} \frac{\mathrm{d}\, p_g}{\mathrm{d}\, t} = v_{g\alpha} \frac{\mathrm{d}\, i_{f\alpha}}{\mathrm{d}\, t} + \mathrm{i}_{f\alpha} \frac{\mathrm{d}\, v_{g\alpha}}{\mathrm{d}\, t} + v_{g\beta} \frac{\mathrm{d}\, i_{f\beta}}{\mathrm{d}\, t} + i_{f\beta} \frac{\mathrm{d}\, v_{g\beta}}{\mathrm{d}\, t} \\ \frac{\mathrm{d}\, q_g}{\mathrm{d}\, t} = v_{g\beta} \frac{\mathrm{d}\, i_{f\alpha}}{\mathrm{d}\, t} + i_{f\alpha} \frac{\mathrm{d}\, v_{g\beta}}{\mathrm{d}\, t} - v_{g\alpha} \frac{\mathrm{d}\, i_{f\beta}}{\mathrm{d}\, t} + i_{f\beta} \frac{\mathrm{d}\, v_{g\alpha}}{\mathrm{d}\, t} \end{cases}. \quad (8)$$

These power dynamics are influenced by the FLVSI inject current and grid voltage dynamics. To simplify these dynamics, we assume that the grid voltage is balanced. Thus, the grid voltage in the αβ0-frame can be obtained as:

$$\begin{cases} v_{g\alpha} = V_{g\max} \cos(\omega t) \\ v_{g\beta} = V_{g\max} \sin(\omega t) \\ v_{g0} = 0 \end{cases}, \quad (9)$$

where $V_{g\max} = \sqrt{v_{g\alpha}^2 + v_{g\beta}^2}$ is the grid voltage magnitude.

The grid voltage dynamics in the αβ0-frame are obtained by the derivative of Eq. (9), as follows:

$$\begin{cases} \frac{\mathrm{d} v_{g\alpha}}{\mathrm{d} t} = -\omega V_{g\max} \sin(\omega t) = -\omega v_{g\beta} \\ \frac{\mathrm{d} v_{g\beta}}{\mathrm{d} t} = \omega V_{g\max} \cos(\omega t) = \omega v_{g\alpha} \end{cases}. \quad (10)$$

Substituting Eq. (5), Eq. (7), and Eq. (10) into Eq. (8), the grid power dynamics in Eq. (8) become [32]:

$$\begin{cases} \frac{\mathrm{d}\, p_g}{\mathrm{d}\, t} = -\frac{R_f}{L_f} p_g - \omega q_g + \frac{1}{L_f} (v_{g\alpha} v_{f\alpha} + v_{g\beta} v_{f\beta} - V_{g\max}^2) \\ \frac{\mathrm{d}\, q_g}{\mathrm{d}\, t} = \omega p_g - \frac{R_f}{L_f} q_g + \frac{1}{L_f} (v_{g\beta} v_{f\alpha} - v_{g\alpha} v_{f\beta}) \end{cases}. \quad (11)$$

It can be observed from Eq. (11) that the grid power dynamics model is a multi-input multi-output (MIMO) system in which the FLVSI output voltages $v_{f\alpha}$ and $v_{f\beta}$ are the original control inputs and the grid powers p_g and q_g are the outputs. We also observed that the grid power dynamics are a time-varying (TV) system, where the control inputs $v_{f\alpha}$ and $v_{f\beta}$ are multiplied simultaneously by the grid voltages $v_{g\alpha}$ and $v_{g\beta}$. To simplify this power dynamics model, we are introducing the following new control inputs, v_p and v_q as follows:

$$\begin{cases} v_p = v_{g\alpha} v_{f\alpha} + v_{g\beta} v_{f\beta} \\ v_q = v_{g\beta} v_{f\alpha} - v_{g\alpha} v_{f\beta} \end{cases}. \quad (12)$$

By using the grid voltages given in Eq. (9), the new control inputs v_p and v_q given in Eq. (12) are changed into *dc* components as follows:

$$\begin{bmatrix} v_p \\ v_q \end{bmatrix} = V_{g\max} \begin{bmatrix} \cos(\omega t) & \sin(\omega t) \\ \sin(\omega t) & -\cos(\omega t) \end{bmatrix} \begin{bmatrix} v_{f\alpha} \\ v_{f\beta} \end{bmatrix} = V_{g\max} \begin{bmatrix} v_{fd} \\ v_{fq} \end{bmatrix}, \quad (13)$$

where v_{fd} and v_{fq} are the FLVSI output voltages in the dq0-frame, which are obtained through the new control inputs in Eq. (13) without using the synchronization method and Park transformation.

Using these new control inputs, the grid power dynamics model in Eq. (11) becomes:

$$\begin{cases} \frac{\mathrm{d}\, p_g}{\mathrm{d}\, t} = -\frac{R_f}{L_f} p_g - \omega q_g + \frac{1}{L_f} (v_p - V_{g\max}^2) \\ \frac{\mathrm{d}\, q_g}{\mathrm{d}\, t} = \omega p_g - \frac{R_f}{L_f} q_g + \frac{1}{L_f} v_q \end{cases}. \quad (14)$$

Note that the inject power dynamics in Eq. (14) are a MIMO and a time-invariant (TI) system with a coupling effect between active and reactive powers and have the same structure as the FLVSI inject current dynamics in the dq0-frame given in Eq. (3). Then, we will present the relationship between these dynamics. The grid active and reactive powers can be expressed in the dq-frame as follows:

$$\begin{cases} p_g = \mathrm{v}_{gd} i_{fd} + \mathrm{v}_{fq} i_{fq} \\ q_g = -\mathrm{v}_{gd} i_{fq} + \mathrm{v}_{fq} i_{fd} \end{cases}. \quad (15)$$

In the dq0-frame, when v_{gd} is oriented to the grid voltage vector and v_{gq} is in quadrature with it, $v_{gd} = V_{g\max}$ and $v_{gq} = 0$, the grid powers in Eq. (15) become:

$$\begin{cases} p_g = V_{g\max} i_{fd} \\ q_g = -V_{g\max} i_{fq} \end{cases}. \quad (16)$$

Substituting Eq. (16) into Eq. (14) and using Eq. (13), the new dq-axes FLVSI inject current dynamics can be derived from the grid power dynamics model as follows:

$$\begin{cases} \dfrac{\mathrm{d}i_{fd}}{\mathrm{d}t} = -\dfrac{R_f}{L_f} i_{fd} + \omega i_{fq} - \dfrac{V_{g\max}}{L_f} + \dfrac{v_{fd}}{L_f} \\ \dfrac{\mathrm{d}i_{fq}}{\mathrm{d}t} = -\dfrac{R_f}{L_f} i_{fq} - \omega i_{fd} + \dfrac{v_{fq}}{L_{f\ L}} \end{cases} . \tag{17}$$

Note that the proposed new dq-axes FLVSI inject current dynamics in Eq. (11) are changed into traditional dq-axes FLVSI inject current dynamics without using the synchronization method and Park transformation.

By considering the zero-sequence input current dynamic (Di_{f0}/dt), the new dq-axes FLVSI inject current dynamics model in Eq. (17) becomes:

$$\begin{cases} \dfrac{\mathrm{d}i_{fd}}{\mathrm{d}t} = -\dfrac{R_f}{L_f} i_{fd} + \omega i_{fq} - \dfrac{V_{g\max}}{L_f} + \dfrac{v_{fd}}{L_f} \\ \dfrac{\mathrm{d}i_{fq}}{\mathrm{d}t} = -\dfrac{R_f}{L_f} i_{fq} - \omega i_{fd} + \dfrac{v_{fq}}{L_f} \\ \dfrac{\mathrm{d}i_{f0}}{\mathrm{d}t} = -\dfrac{(R_f + 3L_n)}{(L_f + 3L_n)} i_{f0} - \dfrac{v_{g0} + v_{f0}}{(L_f + 3L_n)} \end{cases} . \tag{18}$$

We can observe that the new dq0-axes FLVSI inject current dynamics model in Eq. (18) derived from the grid active and reactive power theory without using any synchronization method and Park transformation is almost the traditional model in Eq. (3) obtained from Park transformation using the PLL.

3 Improved VOC strategy for grid connected four leg PWM VSI

Figs. 2 and 3 show both traditional VOC and proposed IVOC schematics for the GC-FLVSI controlled using linear PI controllers in the dq0-frame, respectively. As shown in Fig. 2, the traditional VOC structure is formed using PLL, some parks transformation, and inject current controllers, while the proposed IVOC structure has no PLL and no Parks transformation, which is based on the DPC concept to determine the dq0-axes inject currents and dq0-axes grid voltages and to synchronize the GC-FLVSI system as shown in Fig. 3.

3.1 Current controller of both control strategies

In this section, both control strategies, traditional VOC and the proposed IVOC based on a simple linear PI controller of grid-connected four leg PWM VSI in the dq0-frame, are represented and analyzed.

$$\begin{cases} u_d = (L_f \dfrac{\mathrm{d}i_{fd}}{\mathrm{d}t} + R_f i_{fd}) \\ u_q = (L_f \dfrac{\mathrm{d}i_{fq}}{\mathrm{d}t} + R_f i_{fq}) \\ u_0 = ((L_f + 3L_n) \dfrac{\mathrm{d}i_{f0}}{\mathrm{d}t} + (R_f + 3R_n) i_{f0}) \end{cases} \tag{19}$$

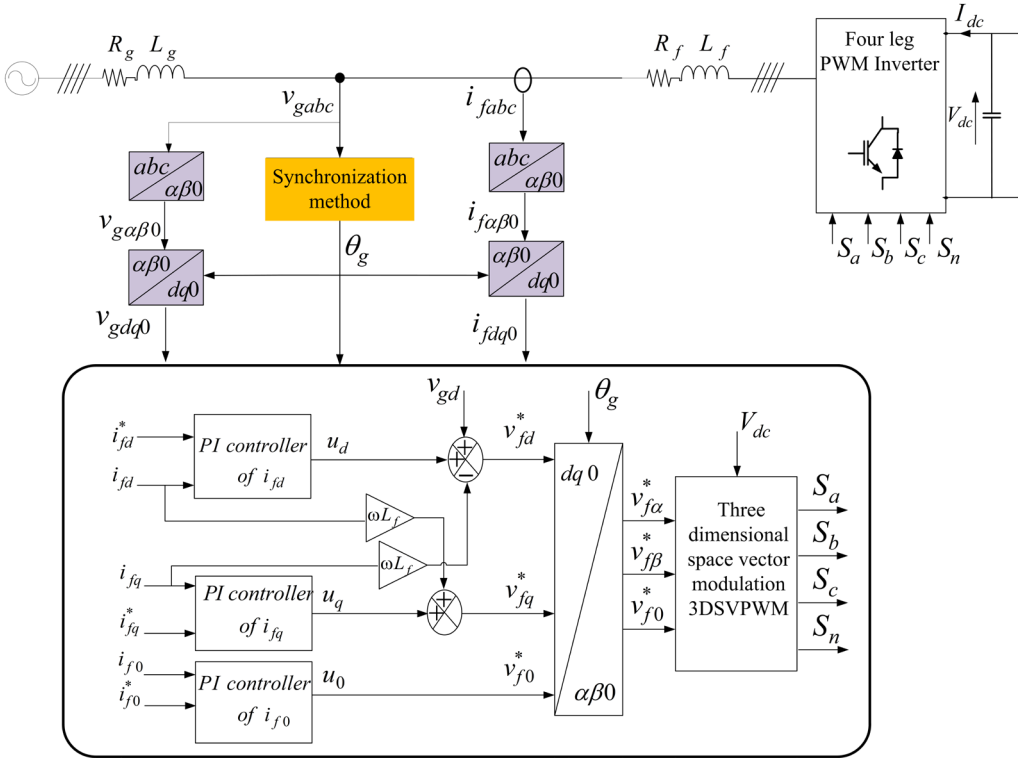

Fig. 2 Traditional VOC circuit schematic of the three-phase grid-connected four leg PWM VSI

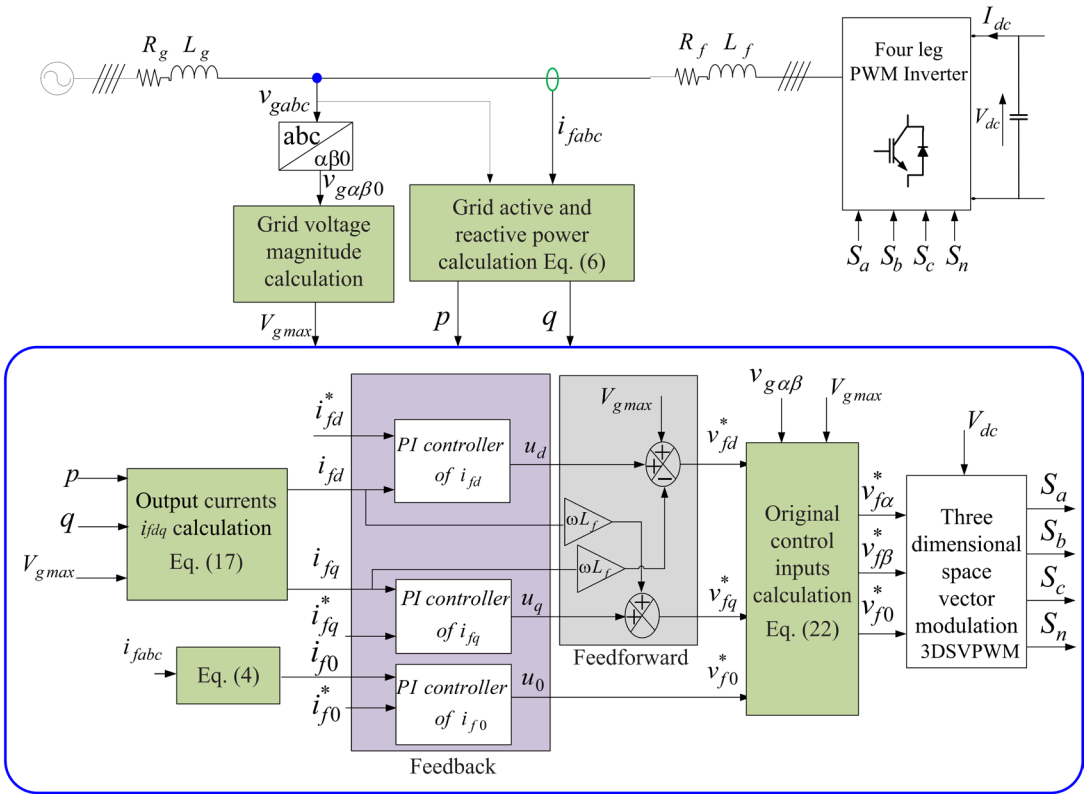

Fig. 3 Proposed IVOC circuit schematic of the three-phase grid-connected four leg PWM VSI

According to Eq. (19), there are coupling terms between the d-axis output current i_{fd} and the q-axis output current i_{fq}. These coupling terms are mitigated by the introduction of decoupling control variables (u_d and u_q) as follows:

The FLVSI output voltages, or the control inputs v_{fdq0} in the dq0-frame, are given as:

$$\begin{cases} \underbrace{v_{fd}^*}_{\text{feedback}} = u_d - \underbrace{\omega L_f i_{fq} + V_{g\max}}_{\text{feedforward}} \\ \underbrace{v_{fq}^*}_{\text{feedback}} = u_q + \underbrace{\omega L_f i_{fd}}_{\text{feedforward}} \\ v_{f0}^* = u_0 \end{cases}. \tag{20}$$

Using the inverse of Eq. (9) and the control inputs v_{fdq0} in Eq. (20), the original control inputs $v_{f\alpha\beta0}$ in the αβ0-frame can be expressed as:

$$\begin{bmatrix} v_{f\alpha}^* \\ v_{f\beta}^* \\ v_{f0}^* \end{bmatrix} = \frac{1}{V_{g\max}} \begin{bmatrix} v_{g\alpha} & v_{g\beta} & 0 \\ v_{g\beta} & -v_{g\alpha} & 0 \\ 0 & 0 & 1 \end{bmatrix} \begin{bmatrix} v_{fd}^* \\ v_{fq}^* \\ v_{f0}^* \end{bmatrix}. \tag{21}$$

From these system equations, it is clear that the d-axis output current i_{fd} and the q-axis output current i_{fq} can be regulated by the decoupled control variables u_d and u_q separately.

The output control variables of the PICs used in the three current inner loops of both control strategies are given in the subsequent expression:

$$u_{dq0} = (k_{p-idq0} + \frac{k_{i-idq0}}{s})(i_{fdq0} - i_{fdq0}^*), \tag{22}$$

where k_p and k_i are the proportional and integral gains of the PICs, which are calculated using the pole placement method as follows:

$$\begin{cases} k_{p-idq} = 2L_f \xi_i \acute{E}_{c-i} - R_f \\ k_{i-idq} = L_f \omega_{c-i}^2 \end{cases}, \tag{23}$$

$$\begin{cases} k_{p-i0} = 2(L_f + 3L_n)\xi_i \acute{E}_{c-i} - (R_f + 3R_n) \\ k_{i-i0} = (L_f + 3L_n)\omega_{c-i}^2 \end{cases}, \tag{24}$$

where ω_{c-i} and ξ_i are the cut-off angular frequency and the damping factor of PIC, respectively. The damping factor is chosen as ξ_i = 0.707 for appropriate overshoot under a transient process. And the cut-off angular frequency is chosen as ω_{c-I} = 3500 rad/s for the adjustment between dynamic responses and immunity versus distortion and harmonic currents.

4 Test studies

In order to investigate the control performance and dynamic response of the proposed IVOC strategy, the simulations

of the grid-connected four-leg VSI system shown in Fig. 1 are achieved in MATLAB/Simulink under balanced and unbalanced grid voltage conditions. The parameters of the grid-connected four-leg VSI control system and simulation are presented in Table 1.

The simulation scenarios chosen for the control performance and dynamic response evaluation are the dq-axes four leg PWM VSI inject current variations as well as output active and reactive power variations under both balanced and unbalanced grid voltages. In addition, to further demonstrate the performance of the proposed IVOC strategy, simulation scenarios in which the PI_{pll} natural frequency ω_{pll} is varied are achieved under traditional VOC strategies, and the output active and reactive powers are analyzed.

Firstly, a comparative study between the proposed IVOC and traditional VOC strategies under a balanced grid voltage case In the first scenario of this case, the reference of i_{fd} is set to 5 A, and the references of i_{fq0} are set to 0 A (p set to 1350 W and q set to 0 VAR) is performed, as shown in Figs. 4 and 5. The waveforms of both figures, from top to bottom, respectively, are: a) three-phase grid voltages; b) three-phase and neutral grid currents; c) dq-axes four leg PWM VSI inject currents; d) zero-sequence current; e) grid active and reactive power.

The second scenario of this case is that the reference of i_{fd} is changed from 5 to 10 A at t = 0.05 s and the references of i_{fq0} are set to 0A (p change from 1350 to 2700 W and q set to 0 VAR). The results of both strategies in this scenario are depicted in Figs. 6 and 7.

The results of the third scenario, when the reference of i_{fq} is changed from -5 to 5 A at t = 0.05 s and the references of i_{fd0} are set to 0 A (q changed from -1350 to 1350 VAR at t = 0.05 s and p set to 0 W), are illustrated in Figs. 8 and 9.

The fourth and final scenario of this case is that the ifd is changed from 0 to 5 A at t = 0.05 s and the i_{fq} is changed from 0 to -5 A at t = 0.1 s, and the results of both control strategies are illustrated in Figs. 10 and 11. The waveforms of both figures in each of the last three scenarios, from top to bottom, are, respectively: a) three-phase and neutral grid currents; b) grid active and reactive power; and d) first-phase grid current and its corresponding voltage.

It can be observed from these four scenarios that the control performance of the proposed IVOC strategy for grid-connected four-leg PWM VSI under different changes

Table 1 Values of system and simulation parameters

Parameter	Value
AC grid voltage	220 V
Fundamental frequency of grid voltage	50 Hz
DC-bus voltage, V_{dc}	650 V
Input filter inductances, L_f, L_{fn}	2 mH, 1 mH
Input filter resistances, R_f, R_{fn}	0.15 Ω
Grid inductances, L_g, L_{gn}	0.1 mH, 0.05 mH
Sampling period of simulation	10^{-6} s
Switching frequency, f_s	16 kHz

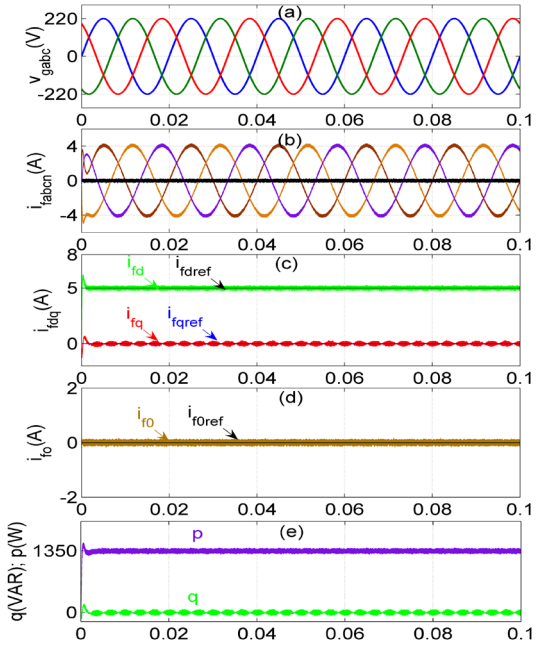

Fig. 4 Performance of the grid-connected four-leg PWM VSI controlled by traditional VOC strategy

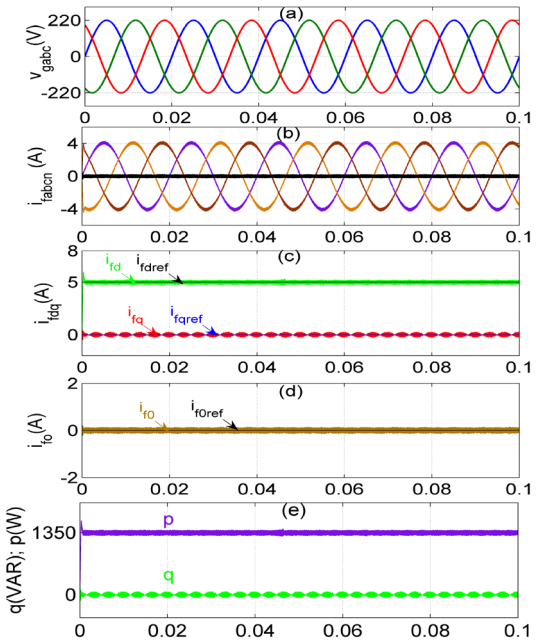

Fig. 5 Performance of the grid-connected four-leg PWM VSI controlled by proposed IVOC strategy

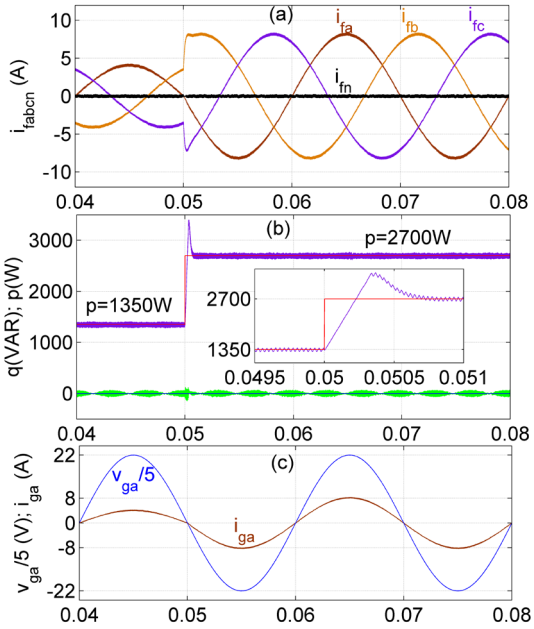

Fig. 6 Dynamic response of the GC-FLVSI using traditional VOC strategy when p changes from 1350 to 2700 W at 0.05 s

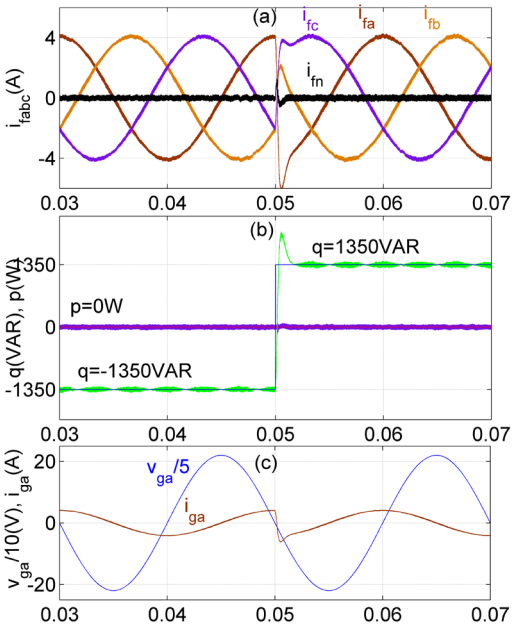

Fig. 8 Dynamic response of the GC-FLVSI using traditional VOC strategy when q changes from -1350 to 1350 VAR at 0.05 s

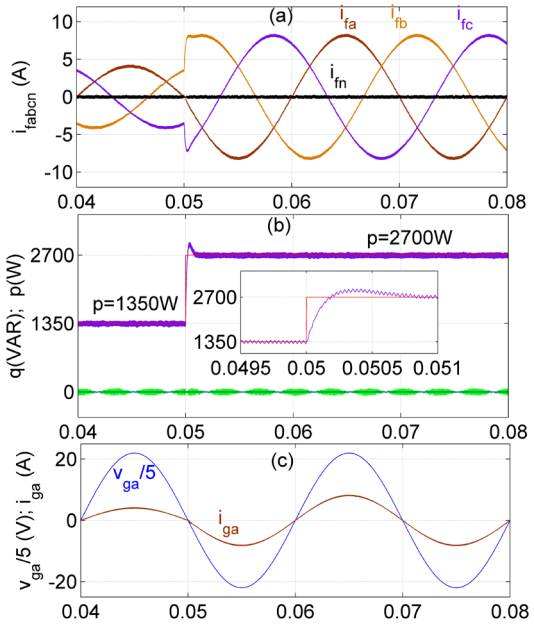

Fig. 7 Dynamic response of the GC-FLVSI using proposed IVOC strategy when p changes from 1350 to 2700 W at 0.05 s

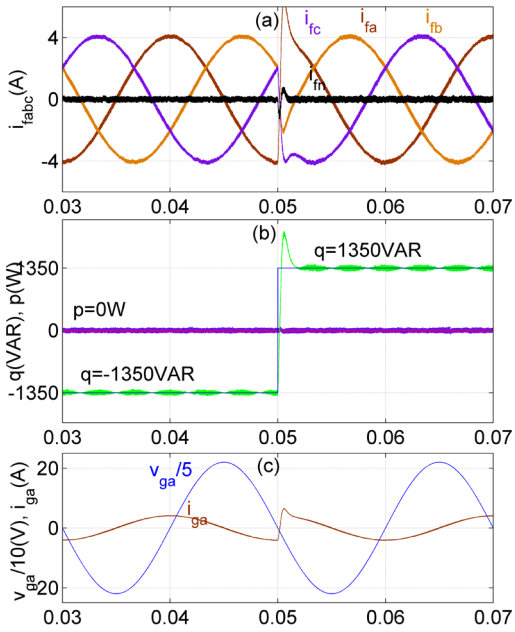

Fig. 9 Dynamic response of the GC-FLVSI using proposed IVOC strategy when q changes from -1350 to 1350 VAR at 0.05 s

of current references in terms of settling times, tracking references, overshoots, and steady-state errors is identical to that of the traditional VOC strategy, since the grid voltage phase angle is correctly detected by the PLL. In addition, the dynamic responses of the grid-connected four-leg PWM VSI with both control strategies are identical as well, because PLL in the traditional VOC strategy does not lose the phase angle information in these scenarios.

So, according to these results, we can conclude that when the grid voltage is balanced, the proposed IVOC strategy has good control performance and dynamic responses with lower computational complexity than the traditional VOC strategy.

In addition to the balanced grid voltage case, the unbalanced grid voltage is also carried in order to examine the control performance of the proposed IVOC strategy in disturbance grid conditions.

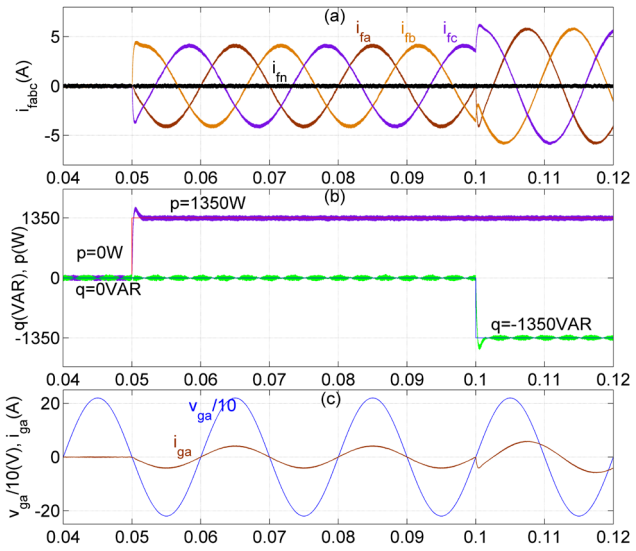

Fig. 10 Dynamic response of GC-FLVSI using VOC when p changes from 0 to 1350 W at 0.05 s and q change from 0 to -1350 VAR at 0.1 s

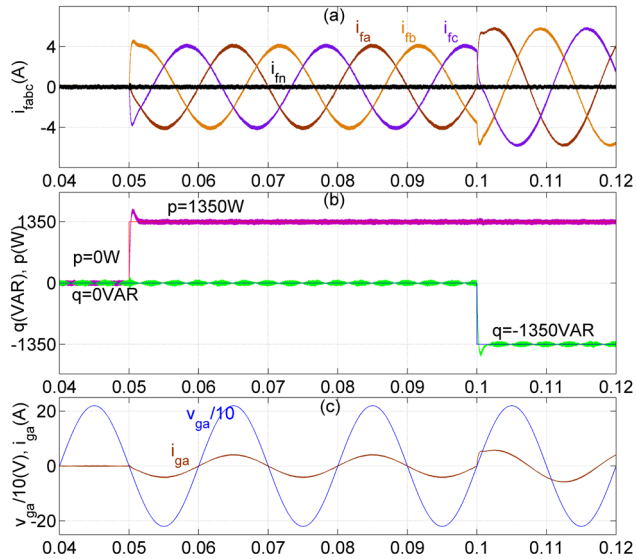

Fig. 11 Dynamic response of the GC-FLVSI using proposed IVOC strategy when p change from 0 to 1350W at 0.05 s and q change from 0 to -1350VAR at 0.1 s

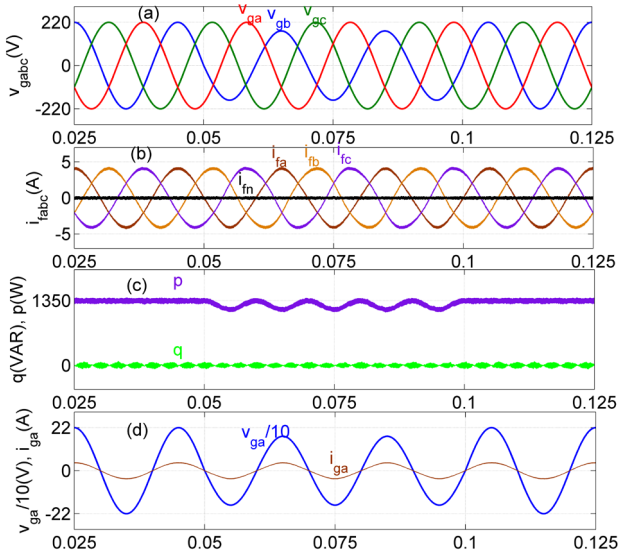

Fig. 12 Dynamic response of the GC-FLVSI using traditional VOC strategy when the first-phase grid voltage has 20 % sag at 0.05 to 0.1 s

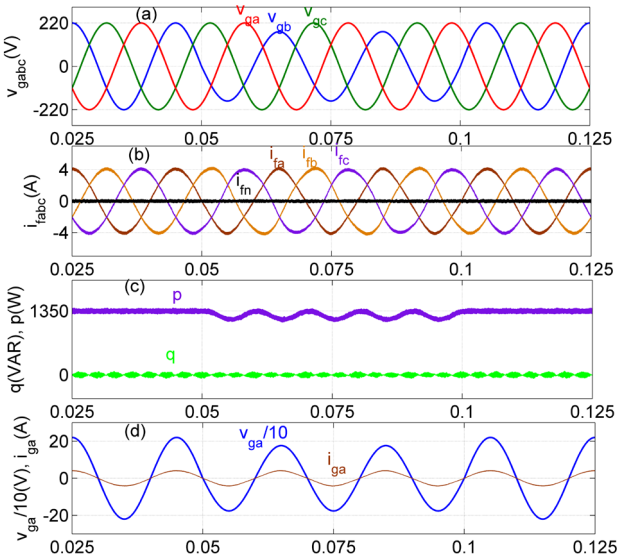

Fig. 13 Dynamic response of the GC-FLVSI using proposed IVOC strategy when the first-phase grid voltage has 20 % sag at 0.05 to 0.1 s

In the first scenario of this case, a comparative study between the proposed IVOC and traditional VOC strategies is performed when the first-phase grid voltage has 20% sag at 0.05 to 0.1 s, as shown in Figs. 12 and 13. The waveforms of both figures, from top to bottom, respectively, are: a) three-phase grid voltages; b) three-phase and neutral grid currents; (c) grid active and reactive power; and (d) first-phase grid current and its corresponding voltage. It is observed from these results that the proposed IVOC strategy has identical control performance and dynamic responses to the traditional VOC strategy, because the PLL in the traditional VOC strategy does not lose the phase angle information in this scenario. Even under this scenario test, the proposed IVOC strategy achieves the current and power control objectives and does not subject the GC-FLVSI system to instability.

We can anticipate that the proposed IVOC strategy will be easily applied to unbalanced grid voltage and will perform well in this scenario.

The second scenario of the unbalanced grid voltage case is that the grid voltages have a 20 % rising amplitude change at 0.05 to 0.1 s, and the results of both control strategies for this scenario are depicted in Figs. 14 and 15. The waveforms of both figures, from top to bottom, respectively, are:

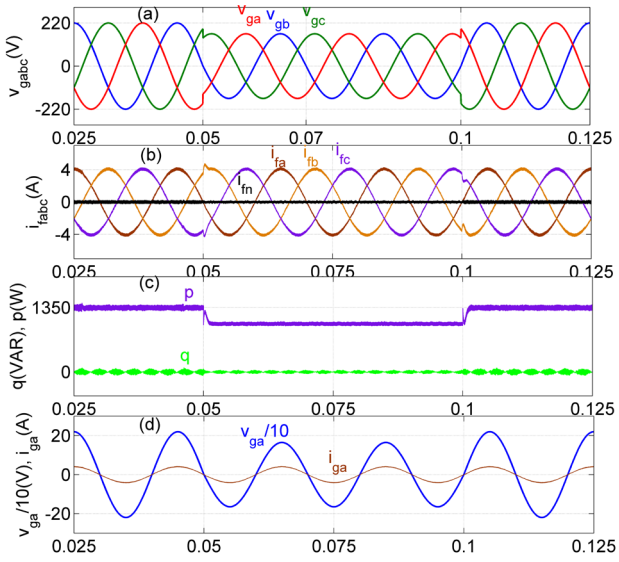

Fig. 14 Dynamic response of the GC-FLVSI using traditional VOC strategy when 20 % rising change in grid voltages at 0.05 to 0.1 s

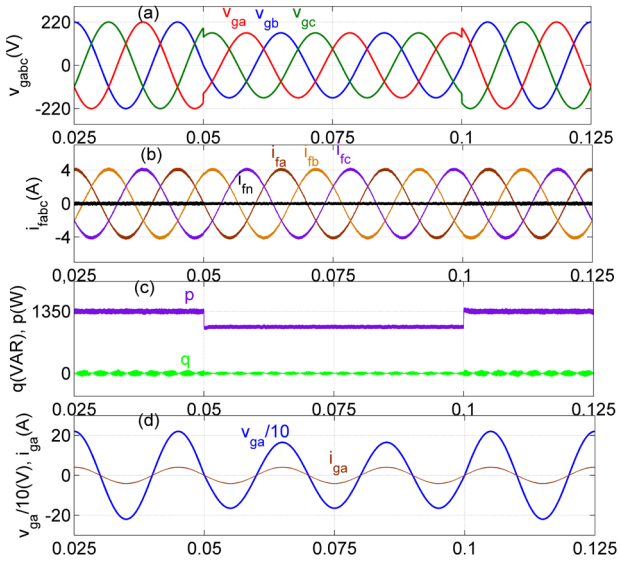

Fig. 15 Dynamic response of the GC-FLVSI using proposed IVOC strategy when 20 % rising change in grid voltages at 0.05 to 0.1 s

a) three-phase grid voltages; b) three-phase and neutral grid currents; (c) injected active and reactive powers; (d) first-phase grid current and its corresponding voltage.

It is observed from these results that both control strategies have almost identical control performance and dynamic responses. Even under these scenario tests, the proposed IVOC strategy meets the current and power control objectives and does not permit the GC-FLVSI system to instability.

To further demonstrate the proposed IVOC strategy performance, a lower PIp_{ll} natural frequency values scenario is considered. Fig. 16 shows the active and reactive power responses for both VOC strategies when the dynamic of the PLL is deteriorated by the decreasing of PIp_{ll} frequency value in the traditional VOC strategy.

In this scenario, when the PIp_{ll} natural frequency value is decreasing, the phase angle is not correctly detected, and the traditional VOC strategy has been influenced. So, the decreases of ω_{pll} impact the increases in settling time and overshoot as well as decrease stability compared to the proposed IVOC strategy, which does not need the PLL. We can conclude that the proposed IVOC strategy has better control performance and dynamic responses than the traditional VOC strategy when the PLL causes any problems.

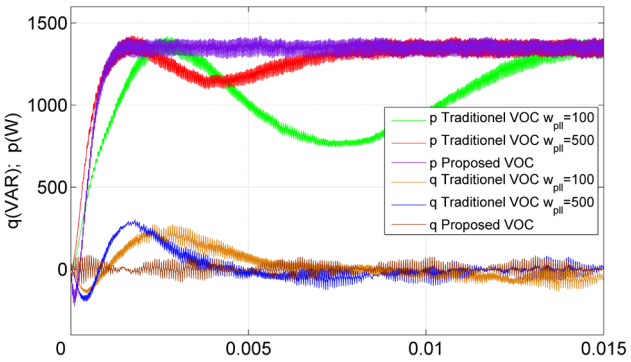

Fig. 16 Grid active and reactive power responses

5 Conclusions

An improved Vector Oriented Control (VOC) strategy in the dq0-frame without synchronization method and Parks transformation for a grid-connected three-phase four leg inverter has been presented. The control performance in terms of settling times, tracking references, overshoots, and steady-state errors is achieved at both balanced and unbalanced grid voltages. This proposed IVOC strategy is not only used for grid-connected four leg inverter synchronization and control but also to provide a linearly time-invariant system in the dq0-frame based on the instantaneous active and reactive powers theory (DPC). This proposed IVOC strategy is validated in a wide range of scenarios through MATLAB/Simulink. Moreover, the proposed IVOC strategy has been compared to a traditional VOC strategy. In contrast to the traditional VOC strategy, the proposed IVOC strategy can achieve identical performance and dynamic responses under both balanced and unbalanced grid voltage without requiring the synchronization method or Parks transformation but will have high performance in several cases where the traditional VOC strategy's bandwidth or natural frequency of PLL causes any problems. We can anticipate, in summary, the following features and advantages of the proposed IVOC strategy:

1. The proposed IVOC strategy does not need Parks transformation to provide a linear time-invariant GC-VSI system in the dq0-frame and can be provided using the instantaneous active and reactive powers theory (DPC).
2. The proposed IVOC strategy does not need a synchronization method, and Parks transformation and its frequency could track the grid voltage frequency easily.
3. The proposed IVOC strategy has a simple structure and lower complexity.

References

[1] Guidara, I., Souissi, A., Chaabene, M. "Novel configuration and optimum energy flow management of a grid-connected photovoltaic battery installation", Computers & Electrical Engineering, 85, 106677, 2020.
https://doi.org/10.1016/j.compeleceng.2020.106677

[2] Oubbati, B. K., Boutoubat, M., Rabhi, A., Belkheiri, M. "Experiential integral backstepping sliding mode controller to achieve the maximum power point of a PV system"", Control Engineering Practice, 102, 104570, 2020.
https://doi.org/10.1016/j.conengprac.2020.104570

[3] Berkani, Y., Taib, N. "Dual Input Z-source Indirect Matrix Converter for Grid Connected Hybrid Renewable Energy Systems", Periodica Polytechnica Electrical Engineering and Computer Science, 65(3), pp. 218–226, 2021.
https://doi.org/10.3311/PPee.18031

[4] Tsang, K. M., Chan, W. L. "Three-level grid-connected photovoltaic inverter with maximum power point tracking", Energy Conversion and Management, 65, pp. 221–227, 2013.
https://doi.org/10.1016/j.enconman.2012.08.008

[5] Ali, Z., Christofides, N., Saleem, K., Polycarpou, A., Mehran, K. "Performance evaluation and benchmarking of PLL algorithms for grid-connected RES applications", IET Renewable Power Generation, 14(1), pp. 52–62, 2020.
https://doi.org/10.1049/iet-rpg.2019.0434

[6] Alali, M. A. E., Sabiri, Z., Shtessel, Y. B., Barbot, J.-P. "Study of a common control strategy for grid-connected shunt active photovoltaic filter without DC/DC converter", Sustainable Energy Technologies and Assessments, 45, 101149, 2021.
https://doi.org/10.1016/j.seta.2021.101149

[7] Malla, S. G., Bhende, C. N. "Voltage control of stand-alone wind and solar energy system", International Journal of Electrical Power & Energy Systems, 56, pp. 361–373, 2014.
https://doi.org/10.1016/j.ijepes.2013.11.030

[8] Venkatasamy, B., Kalaivani, L. "Modeling and Power Quality Analysis of Grid-Connected PV Inverter with Active and Reactive Power Injection Mode", Journal of Electrical Engineering & Technology, 16(3), pp. 1375–1387, 2021.
https://doi.org/10.1007/s42835-021-00693-w

[9] Menaga, D., Sankaranarayanan, V. "A novel nonlinear sliding mode controller for a single stage grid-connected photovoltaic system", ISA Transactions, 107, pp. 329–339, 2020.
https://doi.org/10.1016/j.isatra.2020.07.021

[10] Zhang, R., Lee, F. C., Boroyevich, D. "Four-legged three-phase PFC rectifier with fault tolerant capability", In: Proceedings of the IEEE 31st Annual Power Electronics Specialists Conference, Galway, Ireland, 2000, pp. 359–364. ISBN 0-7803-5692-6
https://doi.org/10.1109/PESC.2000.878878

[11] Kaszewski, A., Galecki, A., Ufnalski, B., Grzesiak, L. M. "State-space current control for four-leg grid-connected PWM rectifiers with active power filtering function", In: Proceedings of the 16th International Power Electronics and Motion Control Conference and Exposition, Antalya, Turkey, 2014, pp. 1265–1271. ISBN 978-1-4799-2060-0
https://doi.org/10.1109/EPEPEMC.2014.6980686

[12] Song, T., Wang, P., Zhang, Y., Gao, F., Tang, Y., Pholboon, S. "Suppression Method of Current Harmonic for Three-Phase PWM Rectifier in EV Charging System", IEEE Transactions on Vehicular Technology, 69(9), pp. 9634–9642, 2020.
https://doi.org/10.1109/TVT.2020.3005173

[13] Carrasco, G., Silva, C. A., Peña, R., Cárdenas, R. "Control of a four-leg converter for the operation of a DFIG feeding stand-alone unbalanced loads", IEEE Transactions on Industrial Electronics, 62(7), pp. 4630–4640, 2015.
https://doi.org/10.1109/TIE.2014.2364155

[14] Chebabhi, A., Fellah, M. K., Kessal, A., Benkhoris, M. F. "A new balancing three level three dimensional space vector modulation strategy for three level neutral point clamped four leg inverter based shunt active power filter controlling by nonlinear back stepping controllers", ISA Transactions, 63, pp. 328–342, 2016.
https://doi.org/10.1016/j.isatra.2016.03.001

[15] Mandrioli, R., Viatkin, A., Hammami, M., Ricco, M., Grandi, G. "A comprehensive AC current ripple analysis and performance enhancement via discontinuous PWM in three-phase four-leg grid-connected inverters", Energies, 13(17), 4352, 2020.
https://doi.org/10.3390/en13174352

[16] Olives-Camps, J. C., Mauricio, J. M., Barragán-Villarejo, M., Matas-Díaz, F. J. "Voltage control of four-leg VSC for power system applications with nonlinear and unbalanced loads", IEEE Transactions on Energy Conversion, 35(2), pp. 640–650, 2020.
https://doi.org/10.1109/TEC.2019.2957185

[17] Chebabhi, A., Fellah, M. K., Kessal, A., Benkhoris, M. F. "Comparative study of reference currents and DC bus voltage control for Three-Phase Four-Wire Four-Leg SAPF to compensate harmonics and reactive power with 3D SVM", ISA Transactions, 57, pp. 360–372, 2015.
https://doi.org/10.1016/j.isatra.2015.01.011

[18] Dheepanchakkravarthy, A., Akhil, S., Venkatraman, K., Selvan, M. P., Moorthi, S. "Performance analysis of FPGA controlled four-leg DSTATCOM for multifarious load compensation in electric distribution system", Engineering Science and Technology, an International Journal, 21(4), pp. 692–703, 2018.
https://doi.org/10.1016/j.jestch.2018.05.004

[19] Chebabhi, A., Fellah, M. K., Kessal, A., Benkhoris, M. F. "Four Leg DSTATCOM based on Synchronous Reference Frame Theory with Enhanced Phase Locked Loop for Compensating a Four Wire Distribution Network under Unbalanced PCC Voltages and Loads", Journal of Power Technologies, 96(1), pp. 15–26, 2016. [online] Available at: https://papers.itc.pw.edu.pl/index.php/JPT/article/view/789

[20] Chebabhi, A., Fellah, M.-K., Benkhoris, M.-F. "3D space vector modulation control of four-leg shunt active power filter using pq0 theory", [pdf] Revue Roumaine des Sciences Techniques, Série Électrotechnique et Énergétique, 60(2), pp. 185–194, 2015. Available at: http://revue.elth.pub.ro/upload/78451808AChebabhi_2_2015_pp185-194.pdf

[21] Li, Z., Zang, C., Zeng, P., Yu, H., Li, S., Bian, J. "Control of a grid-forming inverter based on sliding-mode and mixed H2/H∞ control", IEEE Transactions on Industrial Electronics, 64(5), pp. 3862–3872, 2017. https://doi.org/10.1109/TIE.2016.2636798

[22] Sang, S., Gao, N., Cai, X., Li, R. "A novel power-voltage control strategy for the grid-tied inverter to raise the rated power injection level in a weak grid", IEEE Journal of Emerging and Selected Topics in Power Electronics, 6(1), pp. 219–232, 2018. https://doi.org/10.1109/JESTPE.2017.2715721

[23] Gui, Y., Wang, X., Blaabjerg, F. "Vector current control derived from direct power control for grid-connected inverters", IEEE Transactions on Power Electronics, 34(9), pp. 9224–9235, 2019. https://doi.org/10.1109/TPEL.2018.2883507

[24] Melin, P. E., Guzman, J. I., Hernandez, F. A., Baier, C. R., Muñoz, J. A., Espinoza, J. R., Espinosa, E. E. "Analysis and control strategy for a current-source based D-STATCOM towards minimum losses", International Journal of Electrical Power & Energy Systems, 116, 105532, 2020. https://doi.org/10.1016/j.ijepes.2019.105532

[25] Cao, W., Han, M., Zhang, X., Guan, Y., Guerrero, J. M., Vasquez, J. C. "An Integrated Synchronization and Control Strategy for Parallel-Operated Inverters Based on V-I Droop Characteristics", IEEE Transactions on Power Electronics, 37(5), pp. 5373–5384, 2022. https://doi.org/10.1109/TPEL.2021.3135461

[26] Nian, H., Cheng, P., Zhu, Z. Q. "Coordinated Direct Power Control of DFIG System Without Phase-Locked Loop Under Unbalanced Grid Voltage Conditions", IEEE Transactions on Power Electronics, 31(4), pp. 2905–2918, 2016. https://doi.org/10.1109/TPEL.2015.2453127

[27] Ullah, N., Aziz Al Ahmadi, A. "Variable Structure Back-Stepping Control of Two-stage Three Phase Grid Connected PV Inverter", Periodica Polytechnica Electrical Engineering and Computer Science, 64(3), pp. 239–246, 2020. https://doi.org/10.3311/PPee.15412

[28] Ali, Z., Christofides, N., Hadjidemetriou, L., Kyriakides, E., Yang, Y., Blaabjerg, F. "Three-phase phase-locked loop synchronization algorithms for grid-connected renewable energy systems: A review", Renewable and Sustainable Energy Reviews, 90, pp. 434–452, 2018. https://doi.org/10.1016/j.rser.2018.03.086

[29] Song, Y., Blaabjerg, F. "Analysis of middle frequency resonance in DFIG system considering phase-locked loop", IEEE Transactions on Power Electronics, 33(1), pp. 343–356, 2018. https://doi.org/10.1109/TPEL.2017.2672867

[30] Bimarta, R., Kim, K.-H. "A robust frequency-adaptive current control of a grid-connected inverter based on LMI-LQR under polytopic uncertainties", IEEE Power and Energy Society Section, 8, pp. 28756–28773, 2020. https://doi.org/10.1109/ACCESS.2020.2972028

[31] Yan, S., Yang, Y., Hui, S. Y., Blaabjerg, F. "A review on direct power control of pulsewidth modulation converters", IEEE Transactions on Power Electronics, 36(10), pp. 11984–12007, 2021. https://doi.org/10.1109/TPEL.2021.3070548

[32] Malinowski, M., Jasinski, M., Kazmierkowski, M. P. "Simple direct power control of three-phase PWM rectifier using space-vector modulation (DPC-SVM)", IEEE Transactions on Industrial Electronics, 51(2), pp. 447–454, 2004. https://doi.org/10.1109/TIE.2004.825278

[33] Zhang, Y., Xie, W., Zhang, Y. "Deadbeat direct power control of three-phase pulse-width modulation rectifiers", IET Power Electronics, 7(6), pp. 1340–1346, 2014. https://doi.org/10.1049/iet-pel.2013.0563

[34] Yang, H., Zhang, Y., Liang, J., Liu, J., Zhang, N., Walker, P. D. "Robust deadbeat predictive power control with a discrete-time disturbance observer for PWM rectifiers under unbalanced grid conditions", IEEE Transactions on Power Electronics, 34(1), pp. 287–300, 2019. https://doi.org/10.1109/TPEL.2018.2816742

[35] Bilal Waheed, M., Bhatti, A. R., Amjad, M., Saleem, Y., Niazi, S. A., Khokhar, S. "A simplified model predictive control of four-leg two-level inverter", Electric Power Components and Systems, 47(14–15), pp. 1287–1302, 2019. https://doi.org/10.1080/15325008.2019.1661545

[36] Mohammed Chikouche, T., Hartani, K., Terras, T. "Predictive-DPC Based on Duty Cycle Control of PWM Rectifier under Unbalanced Network", Periodica Polytechnica Electrical Engineering and Computer Science, 66(2), pp. 139–147, 2022. https://doi.org/10.3311/PPee.20048

[37] Zheng, X., Xiao, L., Wang, Z., Lei, Y., Wang, C. "Control strategy without phase-locked loop based on coordinate transformation for three-phase AC/DC converter", IET Power Electronics, 8(9), pp. 1701–1709, 2015. https://doi.org/10.1049/iet-pel.2014.0583

[38] Gui, Y., Xu, Q., Blaabjerg, F., Gong, H. "Sliding mode control with grid voltage modulated DPC for voltage source inverters under distorted grid voltage", CPSS Transactions on Power Electronics and Applications, 4(3), pp. 244–254, 2019. https://doi.org/10.24295/CPSSTPEA.2019.00023

[39] Cheng, P., Wu, C., Ning, F., He, J. "Voltage Modulated DPC Strategy of DFIG Using Extended Power Theory under Unbalanced Grid Voltage Conditions", Energies, 13(22), 6077, 2020. https://doi.org/10.3390/en13226077